Radio Science, Volume 31, Number 2, Pages 263–272, March–April 1996

Implementation of frequency domain interferometry at the SOUSY VHF radar: First results

Phillip B. Chilson and Gerhard Schmidt
Max-Planck-Institut für Aeronomie, Katlenburg-Lindau, Germany

Abstract. Frequency domain interferometry (FDI) provides a means of identifying the altitude and width of atmospheric scattering layers with an increased range resolution over conventional pulsed radar measurements. The technique was first formally introduced in 1987 and has since been used in the study of scattering layers from the lower troposphere to the upper mesosphere. Despite its success, FDI has only been implemented on a few atmospheric radars. We present here the first results of FDI measurements conducted at the sounding system (SOUSY) VHF radar in Germany. The flexibility of the SOUSY radar permits simultaneous sampling of regions of the atmosphere using both single and coded pulses, thus facilitating a comparison of the resulting coherences. We present here FDI data obtained during 14 continuous hours of radar operation. The FDI technique is shown to be capable of consistently predicting the location and thickness of atmospheric scattering layers. Such information is important when studying turbulence, scattering mechanisms, and fine-scale structures in the atmosphere.

Introduction

The range resolution of a conventional pulsed Doppler radar is determined by the duration of its transmitted sampling pulse, which translates into a particular sampling length. For radars making observations of the troposphere and stratosphere the sampling pulse is usually 1–2 μs (150–300 m); however, the pulse length may be even longer for observations of the mesosphere. Kelvin-Helmholtz instabilities, low-frequency buoyancy oscillations, and other processes can produce sharp gradients in the refractive index fields of the atmosphere. The gradients typically result from variations in humidity, temperature, or electron densities and are seen in backscattered radar signals as reflecting layers. It is often impossible to investigate the fine-scale structures of the scattering layers due to the limited range resolution of the pulsed radars. Indeed, high-resolution temperature profiles have recently revealed the existence of strong vertical temperature gradients within thin (typically less than 10 m) sheets in the troposphere and stratosphere [*Dalaudier et al.*, 1994]. The authors further discuss to what extent these sheets are able to contribute to radar echoes.

Paper number 95RS03544.
0048-6604/96/95RS-03544$08.00

Frequency domain interferometry (FDI) was first introduced by *Kudeki and Stitt* [1987] and has been developed as a high-resolution means of investigating thin atmospheric scattering layers. Using FDI, two or more closely spaced, alternating frequencies are used to sample a given volume of space, and a cross-correlation or cross-spectral analysis is then conducted on two of the resulting time series data. If energy is primarily scattered from a single layer that is thinner than the vertical extent of the pulse length, then FDI can be used to estimate its range and thickness. However, if the scatterers are uniformly distributed throughout the sampling volume, then the double-frequency result is identical to that of a single-frequency measurement. FDI has been successfully employed in the study of scattering layers in the troposphere, stratosphere, and mesosphere using several different frequencies [e.g., *Kudeki and Stitt*, 1990; *Palmer et al.*, 1990; *Chu and Franke*, 1991; *Stitt and Kudeki*, 1991; *Franke et al.*, 1992; *Palmer et al.*, 1993].

To apply the technique, one first calculates a correlation coefficient from the time series data representing backscatter recorded at two alternating frequencies f_1 and f_2:

$$S_{12} = \frac{\langle V_1 V_2^* \rangle}{\sqrt{\langle |V_1|^2 \rangle \langle |V_2|^2 \rangle}}. \quad (1)$$

Here V_n represents the voltage samples for the two frequencies, the asterisk denotes a complex conjugate, and angle brackets indicate an ensemble average over a collection of time series points. Alternatively, it is possible to perform the analysis in spectral space, in which case the coherence spectrum is calculated

$$S_{12}(\omega) = \frac{\langle V_1(\omega) V_2(\omega)^* \rangle}{\sqrt{\langle |V_1(\omega)|^2 \rangle \langle |V_2(\omega)|^2 \rangle}}, \tag{2}$$

where now $V_n(\omega)$ is the Fourier transform of the time series data. The important difference between (1) and (2) is that in the latter the coherence and phase become functions of the line-of-sight velocities. Using (2), it is possible to describe a layer's thickness and range as a function of the arrival angle within a pulse volume [*Pan et al.*, 1994]. This is done, however, at the cost of statistical significance for a given sampling time.

In both treatments it is assumed that a single scattering layer is present within the radar pulse volume and that the scatterers composing the layer are vertically distributed via a Gaussian function centered at z_l relative to the center of the sampling volume and having a second central moment σ_l^2. Following the notation of *Franke* [1990], the resulting magnitude and phase of the correlation coefficient can be expressed as

$$|S_{12}| = \exp\left[-\Delta k^2 \frac{2\sigma_r^2}{\sigma_l^2 + 2\sigma_r^2} \sigma_l^2 \right] \tag{3}$$

and

$$\angle S_{12} = 2\Delta k \frac{2\sigma_r^2}{\sigma_l^2 + 2\sigma_r^2} z_l, \tag{4}$$

respectively. The difference in wavenumber between the two frequencies is given by Δk, and σ_r^2 is the second central moment of the range-weighting function. It has been assumed that the radar beam width is sufficiently small to neglect the wave front curvature effects discussed by *Franke* [1990]. The contributions from the range-weighting function, however, should not be neglected unless only very thin scattering layers are being considered. This point is discussed in more detail below.

Using (3) and (4), it is possible to solve for z_l and σ_l. In both the time domain and the frequency domain treatment it is necessary to correct the coherence for noise before calculating the width of a scattering layer [*Kudeki and Stitt*, 1990]. That is, one should make the transformation $|S_{12}| \mapsto [(1 + N_1/S_1)(1 + N_2/S_2)]^{1/2}|S_{12}|$, where N/S is the inverse of the signal-to-noise ratio. A direct correction cannot be made, however, for the phase values $\angle S_{12}$, which results in an enhancement in the statistical phase errors. Furthermore, there may be a systematic bias in the measured phase that leads to a constant offset in the estimated location of a layer. For that reason one refers to the layer locations as relative. Although not performed here, *Kilburn et al.* [1994] have demonstrated a method that can be used to correct for the systematic phase error.

Experimental Description

Nominally, the sounding system (SOUSY) VHF radar (51.66°N, 10.49°E) operates at a frequency of 53.5 MHz. Recently, modifications have been completed to facilitate FDI observations using alternating frequencies of 53.25 and 53.75 MHz. The frequency separation of 500 kHz was chosen to match the 300-m height resolution used during the experiment. That is, assuming a scattering layer is present within the sampling volume, the phase calculated using (4) will assume values between $\pm\pi$ over the range of the sampling volume.

An interesting feature of the experiment was the timing sequence of the radar pulses. A diagram depicting this sequence has been presented in Figure 1. As shown, both single (Sipu) and complementary-coded (CoCo) pulses were transmitted on an alternating basis. The pluses and minuses simply represent the 0° and 180° phase differences, respectively, between the pulses used to remove instrumental biases. A more comprehensive discussion of the coding scheme used at the SOUSY VHF radar is given by *Schmidt et al.* [1979]. The single pulses provided measurements from 1.8 to 7.5 km, and an 8-bit complementary code was used to sample the atmosphere from 3.9 to 15.6 km. This represents a total of 60 sampling volumes: 20 using single pulses and 40 using coded pulses. Note that the region from 3.9 to 7.5 km was common to both. This feature of the experiment allowed us to test the reproducibility of the FDI-estimated layer parameters. Also shown in Figure 1 are the different interpulse periods given in microseconds. A complete cycle of single and coded pulses lasted 1800

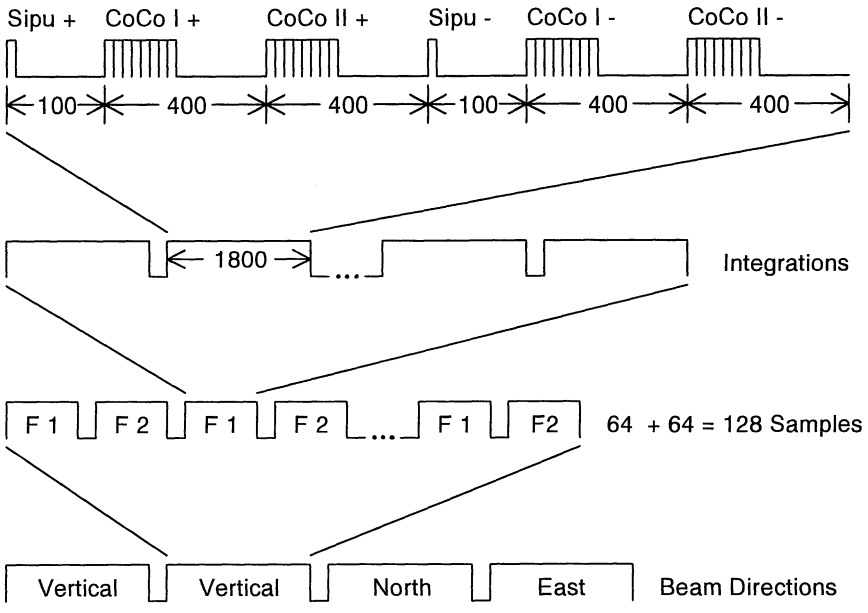

Figure 1. Pulse scheme used by the sounding system (SOUSY) radar during the frequency domain interferometry (FDI) measurements made on October 6, 1994. "Sipu" and "CoCo" indicate the single and complementary-coded pulses, respectively. The times are given in microseconds.

μs, and the sequence was repeated and coherently integrated a number of times before switching to the next frequency. For the measurements described below, 50 coherent integrations were performed yielding a dwell time of 100 ms for each frequency pulse, of which 10 ms was needed for on-line processing.

The radar was cycled through four beam orientations: vertical, vertical, north, and east. A zenith angle of 7° was used for the off-vertical beams. For each beam direction, 128 time series points were collected using alternating frequencies, that is, a total of 64 pulses at 53.25 MHz and a total of 64 pulses at 53.75 MHz. The two sets of 64 time series points were used in computing the cross correlations. Note that two consecutive vertical beam orientations were chosen to provide more data points when performing the correlation calculations. The dwell time for a given beam direction was 12.8 s, and data were transferred to tape after every beam direction.

As seen in (3) and (4), an accurate determination of σ_r is necessary whenever the layer thickness is not very small compared to the pulse length. When Gaussian-matched filters are used in the receiver, σ_r can be approximated by $0.35c\tau/2$, where c is the speed of light in free space and τ is the pulse length in seconds [*Doviak and Zrnić*, 1984]. This yields a value of 105 m for a 2-μs pulse. *Chu and Franke* [1991], however, calculated a value of σ_r for a 2-μs pulse of 55 m for the Chung-Li radar by comparing coherence values for a given altitude range using different frequency separations. Taking advantage of the flexible design of the SOUSY radar, we performed the following test to determine the value of σ_r. A 2-μs pulse was generated in the transmitter and routed through a 100-μs ultrasonic delay line. The attenuated pulse was then fed directly into the receiver unit. Finally, the filtered in-phase and quadrature components of the resulting pulse were displayed on a high-frequency oscilloscope. Through analysis of the digitized scope image we were able to directly determine the value of σ_r to be 95 m.

Having calculated the value for σ_r, we can now investigate the sensitivity of the layer width estimates on the range-weighting function. If an infinite value of σ_r is assumed, then (3) simplifies to $|S_{12}| = \exp[-\Delta k^2 \sigma_l^2]$, which leads to an underestimation of the layer width. Figure 2 shows the amount by which the layer width $2\sigma_l$ will be underestimated as a function of the actual layer width for $\sigma_r = 95$ m. As expected, the degree of underestimation is small for narrow layers but becomes significant for thicker layers. Note that layers having thicknesses

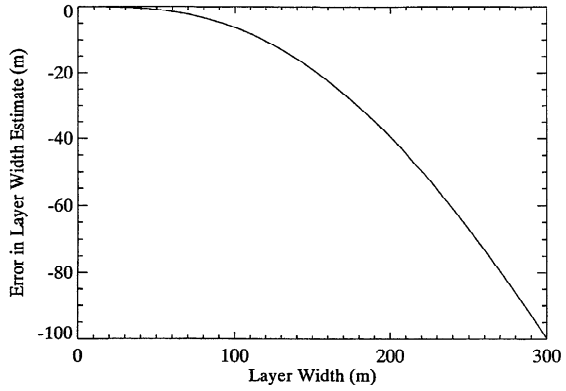

Figure 2. Illustration of the amount the layer width will be underestimated if range-weighting effects are not considered.

of 100 and 150 m will already be underestimated by 6 and 13%, respectively.

Measurements

Observations Without FDI

On October 6 and 7 of 1994, 14 hours (1300–0300 LT) of continuous observations were made at the SOUSY radar using the FDI parameters described above. A few hours before the time of the radar observations the center of a high-pressure system moved almost directly over the radar site, resulting in stable atmospheric conditions. Spectral and correlation analyses were then performed from the resulting time series data. The top panel of Plate 1 shows a range-time-intensity (RTI) plot of the signal-to-noise ratio (snr) calculated using the coded pulses from the vertical beam over the time span of the observations. To obtain the snr values, first two 64-point auto spectra were calculated from each record of 128 time series points, one for each frequency. Then the spectra were incoherently averaged over six radar cycles, that is, 12 incoherent additions for the vertical beam and 6 incoherent averages for the off-vertical beams. Finally, snr values were calculated from each incoherently averaged spectrum separately using its corresponding noise value. These were then averaged for the two frequencies. Hence the figure represents the RTI plot that would result from conventional radar measurements. The vertical bands seen between 10 to 12 km are disturbances in the data, probably resulting from either airplanes or meteor trail echoes in the mesosphere.

Certain features in the RTI plot can be attributed to the atmospheric conditions during the period of the observations. The most striking are the distinct descending layers present below 8 km, possibly indicating subsidence in connection with the high-pressure system that passed over the radar site. For comparison, surface pressure and precipitation data collected at the radar have been included in the bottom panel of Plate 1. Since the time axes for the two plots are different, vertical lines have been included in the lower panel to indicate the start and end times of the radar observations. Note that the radar observations begin just after the peak in the surface pressure and that there was no precipitation during this interval. Although not as evident as the descending layers, a region of enhanced reflectivity having an snr of about 30 dB can also be seen in the RTI plot between 13 and 14 km. This layer persists throughout the observation period and is probably associated with the temperature gradient present near the tropopause.

Sounding profiles were also available [*German Meteorological Service*, 1994] and have been analyzed to examine the vertical structure of the atmosphere during the time of the experiment. A skew-T diagram has been presented in Figure 3, showing data from a radiosonde launched from Hannover (approximately 90 km northwest of the radar) at 1300 LT, during the beginning of the radar observations. Although considerable structure can be seen in the air temperature profile (rightmost curve), the more noticeable feature in the diagram are the sharp spikes in the dew point temperatures (leftmost curve) at approximately 2, 4, and 6.5 km. These represent vertical gradients in humidity, and the location of the spikes indicates the presence of layers of dry air. Sounding data obtained on the next day at 0100 LT also exhibit dry layers but located at 2 and 3.5 km. Consequently, the lower layers in Plate 1 are possibly due to regions of descending humidity gradients. The humidity gradients, however, may not be the only contributing factor to the scattering layers. The layers can also be created by horizontally stratified regions of turbulence. The sounding profiles also reveal the location of the tropopause to be at 12.5 km at 1300 LT and 13.5 km at 0100 LT. These values correspond relatively well with the locations of the upper layer in Plate 1. Note that some deviations in the absolute altitudes of the layers as observed by the radar and

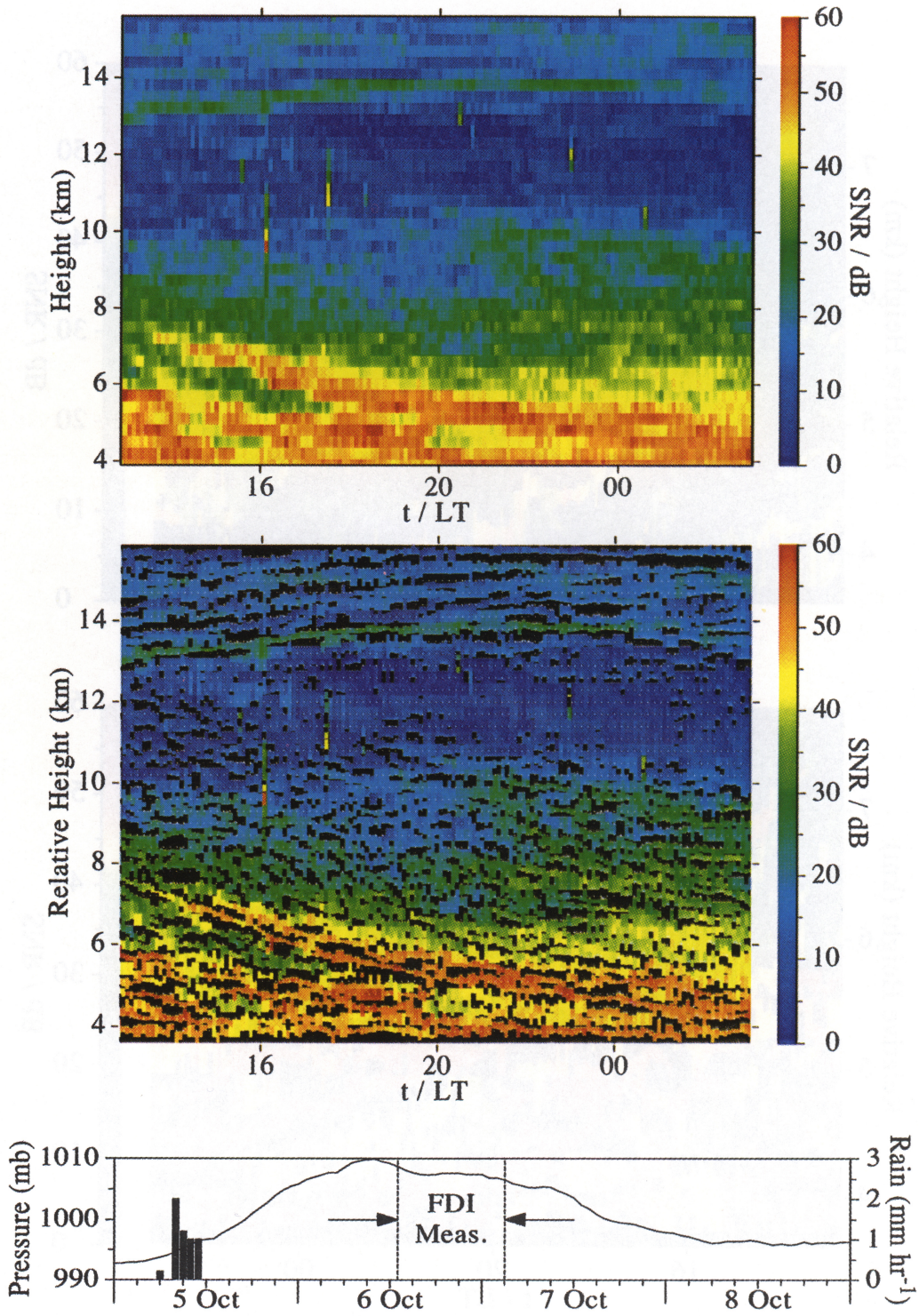

Plate 1. (opposite) (top) Signal-to-noise ratio values obtained from the coded pulses of the vertically oriented beam. The data have been plotted using a conventional range-time-intensity (RTI) plot. (middle) FDI-RTI plot of data shown in top panel, as discussed in the section dealing with FDI observations. (bottom) Barometric pressure and precipitation data acquired at the radar site. The time corresponding to the FDI observations have been indicated by dashed lines.

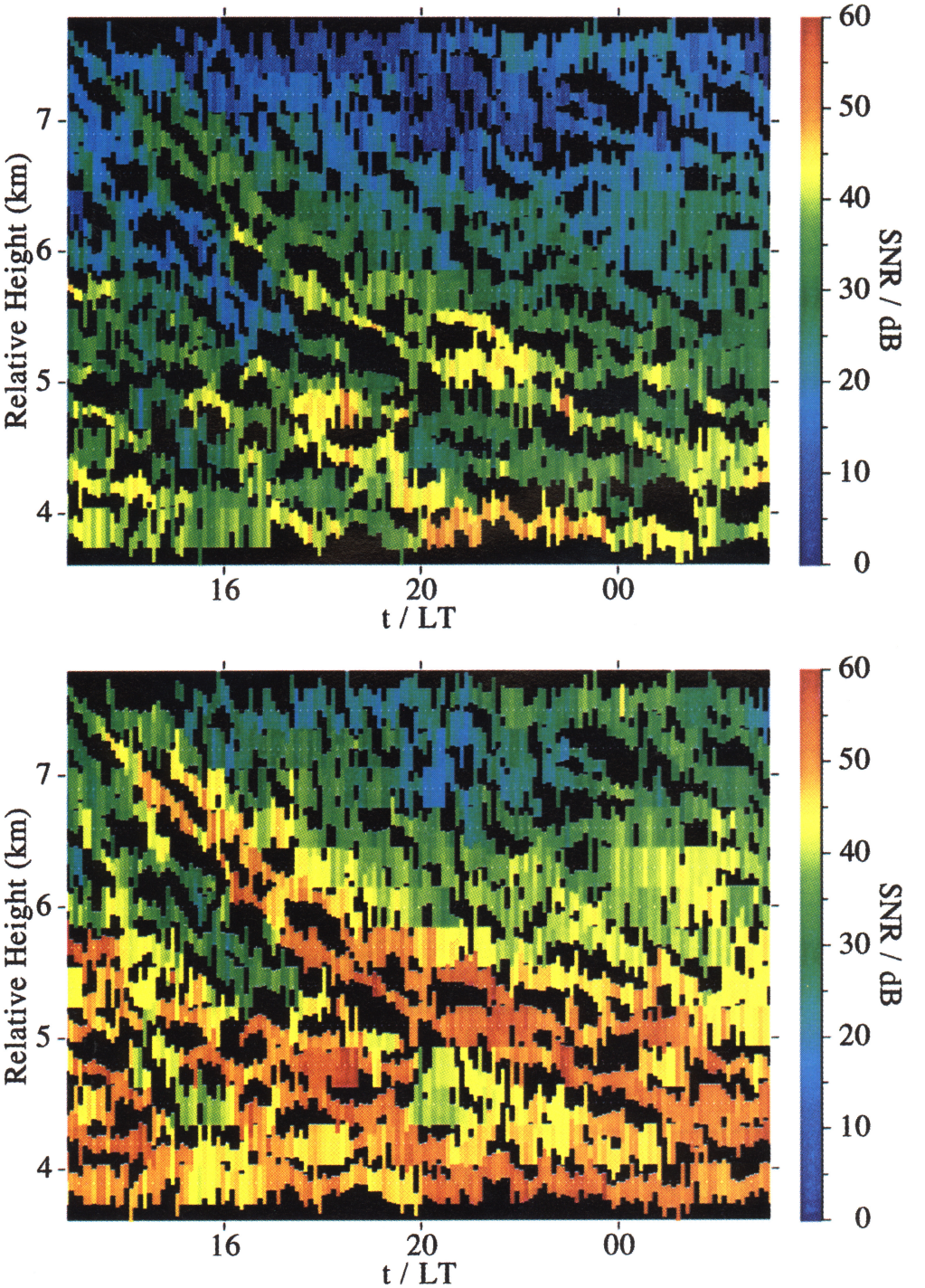

Plate 2. FDI-RTI plots similar to Plate 1 showing the region where the two pulse-coding schemes overlap. The top panel corresponds to single-pulse measurements and the bottom panel shows complementary-coded pulse data.

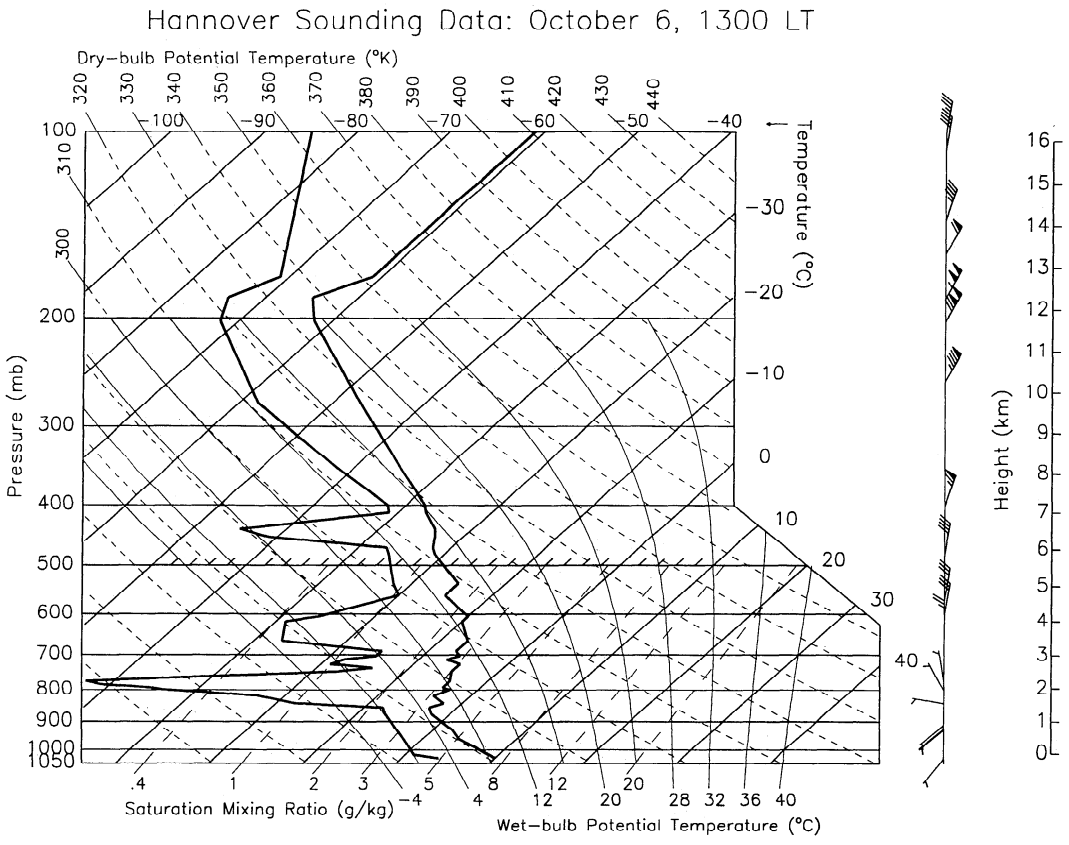

Figure 3. Skew-T diagram showing sounding data from a radiosonde that was launched from Hannover, approximately 90 km northwest of the SOUSY radar site. The rightmost and leftmost curves are for the dry-bulb and dew point temperatures, respectively. Horizontal wind values are shown on the right, where a half barb represents 5 m s^{-1}, a full barb represents 10 m s^{-1}, and a solid triangle is for 50 m s^{-1}.

the sounding are to be expected because of the separation of the two sites.

Observations With FDI

To better investigate the layer structure of the atmosphere during the time of the observations, the FDI treatment of the data will now be presented. First, the complex correlation coefficient was calculated using (1) from the time series data of six radar cycles. An example of the coherence values thus obtained are given in the left-hand panel of Figure 4, where the thick dashed curves show the coherence calculated from the single pulses, and the thick solid curves show the coherence from the coded pulses. As shown in the appendix of *Franke et al.* [1992], the 95% significance level can be calculated with the equation

$$S_{0.95} = [1 - (0.05)^{1/(\nu - 1)}]^{1/2}, \tag{5}$$

where ν is the number of degrees of freedom. The value for ν has been calculated using the equation [*Awe*, 1964]

$$\nu = 1 + \sqrt{\frac{(2 \ln 2)(T/\tau_{1/2})}{\pi}}, \tag{6}$$

where T is the total sampling time and $\tau_{1/2}$ is the lag time of the average correlation function at the half-amplitude point. The value of T was 12(12.8 s) = 153.6 s, and typical values for $\tau_{1/2}$ ranged between roughly 0.5 and 1.5 s. Almost all of the coherence values lie above the 95% significance line, as is also true for the other coherence profiles.

As mentioned earlier, the single-pulse and the

coded-pulse data overlap between 3.9 and 7.5 km and provide quasi-independent methods of observing the same region of the atmosphere. This range interval has been expanded for comparison and is shown in the right-hand panel of Figure 4. Again, the thick dashed curves show the coherence calculated from the single pulses, and thick solid curves show the coherence from the complementary-coded pulses. Here the 95% confidence intervals are shown. The interval was calculated for each coherence value using [*Franke et al.*, 1992]

$$\tanh\,[\operatorname{arctanh}|S_{12}| \pm (1.96/\sqrt{\nu - 1})]. \qquad (7)$$

With the exception of 5.7 km the coherence of the single-pulse and coded-pulse data show very good agreement.

The data have been presented again in the middle panel of Plate 1 using a plotting technique similar to that described by *Palmer et al.* [1990]. In the FDI-RTI plot, only the region between $z_l \pm 2\sigma_l$ for a particular time and range bin is color coded with its corresponding snr value. That is, a scattering layer is said to have a width given by $2\sigma_l$. If no distinct layer is detected, then the entire range and time interval is color coded with the snr value, giving the same result as in the standard RTI plot. The descending layers of the troposphere, as well as the persistent layer near the tropopause, seen in the top panel of Plate 1 are also evident in the FDI-RTI plot but with much clearer detail. In one instance a single layer (located slightly below 8 km at the beginning of the observations) can be seen to descend over several kilometers. This attests to the technique's ability to correctly identify the location of a layer. The layer descends at an average rate of about 10 cm s^{-1}, in line with that expected for subsidence.

As a test of the FDI technique's ability to consistently identify the location and width of scattering layers, FDI-RTI plots similar to the one in the bottom panel of Plate 1 have been created for the region between 3.9 and 7.5 km using both the single-pulse and coded-pulse data. These are shown in Plate 2 with the single-pulse results given in the top panel, and the coded-pulse values shown in the bottom panel. Although the two plots were created using data from different pulse schemes, the results are quite similar. Both the layer widths and locations have been consistently predicted. Note that enhanced snr values are expected for the coded-pulse measurements shown in the bottom panel. Note also that the downward propagation of the scattering layers becomes particularly evident in Plate 2 given the height range chosen for the plots. Since the descent of these layers should also appear in the vertical velocities of the corresponding atmosphere, estimates of the vertical wind obtained from Doppler shifts in the spectra will now be presented.

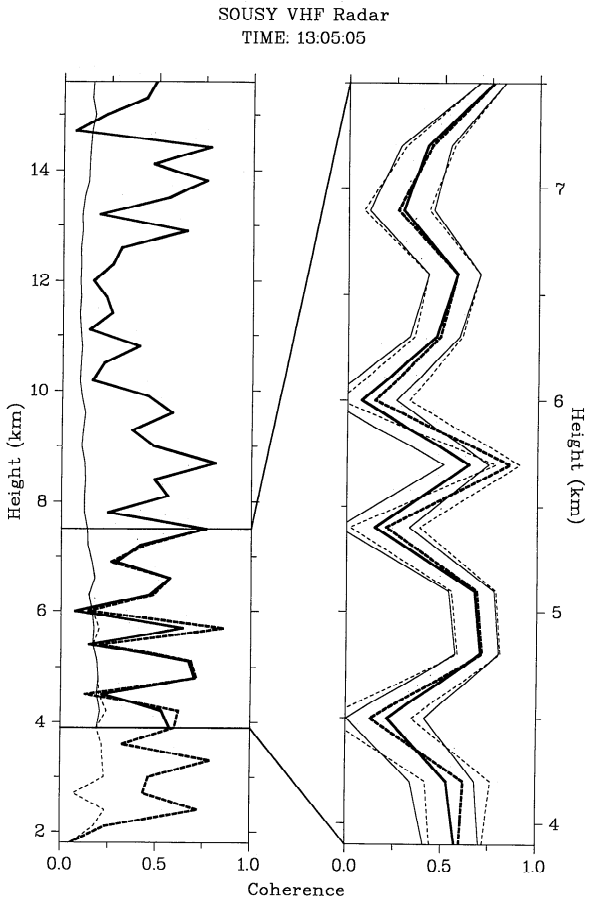

Figure 4. Profiles showing an example of the coherence values (thick curves) obtained over the range of heights used during the experiment. The dashed curves are for the single-pulse values and the solid curves are for the coded-pulse values. The left panel shows the entire coded-pulse range along with the calculated 95% significance level (thin curves). Coherence values for both the single and complementary-coded pulses (thick curves) are shown in the right panel with their 95% confidence intervals (thin curves).

Doppler spectra were formed using the vertical-beam radar data collected over six cycles. First, two 64-point auto spectra were calculated from each record of 128 time series values, one for each

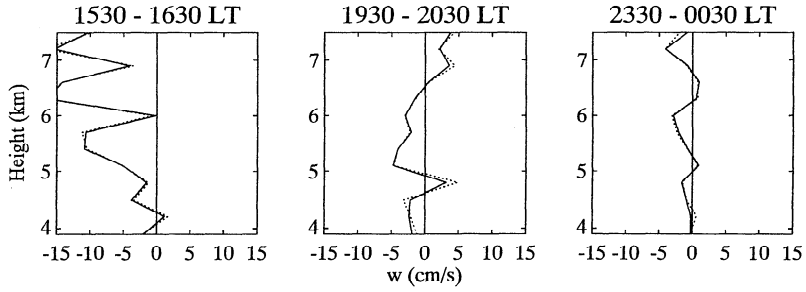

Figure 5. Height profiles of vertical velocities averaged over 1 hour. The three profiles are centered at times 1600, 2000, and 0000 LT. Solid curves have been used to show velocities obtained from the complementary-coded pulses, and dashed curves correspond to the single pulses.

frequency. The spectra for each frequency were then incoherently averaged over the radar cycle, and Doppler velocities were found through the moments method. Finally, the resulting Doppler velocities obtained at both frequencies were averaged together. A plot of the Doppler-estimated vertical winds are shown in Figure 5 as three 1-hour height profiles centered at times 1600, 2000, and 0000 LT. The same height range has been selected for Figure 5 as in Plate 2; therefore, we have wind estimates from both the single-pulse and coded-pulse data, with the former being indicated with a dashed curve and the latter with a solid curve. Both profiles agree very well at all three times.

Examining Plate 2 and Figure 5, we can now compare the descent rate of the scattering layers with the vertical velocity of the atmosphere. The height profile in Figure 5 centered at time 1600 shows the vertical wind to have a value of -15 cm s^{-1} (downward) at heights of approximately 6.3 and 7.1 km. Looking at Plate 2, we find a strong scattering layer having a particularly steep downward slope at a height of 6.3 km and at 1600 LT. Later at 2000 LT the same layer is located at about 5.1 km and is less steeply inclined. Here the corresponding vertical wind is -5 cm s^{-1}. Finally, at midnight the layer is located just below 4.8 km and has almost zero slope. The vertical wind at this height and time, although still downward, only has a value of a few centimeters per second. Therefore it can be said that the position and slope of the scattering layer correlate well with the vertical winds estimated for the atmosphere.

As a final point, the data in Plate 2 can be useful in testing for the existence of false images, as described by *Palmer et al.* [1990]. They pointed out that when strong layers are present and a pulse-coding scheme is used, echoes can be leaked into neighboring range bins. A particular case was shown in their data where a single scattering layer is believed to produce a secondary parallel ghost layer. Such false layers should not be observed when transmitting a single code. Although the scattering layers shown in Plate 2 produce strong echoes, no ghost images have been produced. That is, no layers are present in the bottom panel that cannot likewise be identified in the top panel.

Conclusions

In this article we have presented the first FDI results from the SOUSY VHF radar. Measurements were made during a period when scattering layers were present in both the troposphere and the stratosphere. Sounding profiles were used to study the vertical structure of the atmosphere during the time of the observations, and it was found that the observed scattering layers possibly correspond to gradients in the humidity. Using FDI, it was possible to successfully track the layers even when they were found to descend over several kilometers. To accurately account for the range-weighting effects, a separate measurement was performed to find the second central moment of the range-weighting function for the SOUSY radar when using a 2-μs pulse. An accurate measurement of σ_r is important when calculating both the position and width of a scattering layer.

A unique feature of this experiment has been used to to test the validity of the FDI technique. In particular, the radar parameters were chosen such that a common region of the atmosphere could be simultaneously probed using single and complementary-coded pulses. As a first test, complex

correlation coefficients were calculated for both pulses, and the resulting coherence values were examined in detail. Although the two pulse schemes provide quasi-independent measurements of a common region of the atmosphere, the coherence values were quite similar. Furthermore, estimates of the location and thicknesses of the scattering layers obtained from both the single and complementary-coded pulses showed good agreement. Not only does the agreement lend support to the validity of the FDI method, but it also suggests that the coded-pulse echo power was not leaked into neighboring range bins. Finally, a comparison was made between the downward progression of FDI-estimated layer locations in time and the Doppler-estimated vertical winds. Here, again, good agreement was found.

Although FDI provides a useful tool for studying turbulence, scattering mechanisms, and fine-scale vertical structures in the atmosphere, the technique does need further development. One problem with the FDI technique is its lack of ability to identify more than one scattering layer. If two or more layers exist within a single sampling volume, then the features of the individual layers will be smeared, and the combined contributions will be averaged together. Another problem that needs to be addressed is a validation of the layer estimates produced by the FDI method. We know of no direct comparison of FDI with independent measurements, such as from airplanes or high vertical resolution balloons. Taking these limitations into consideration, the FDI technique offers a simple means of increasing the range resolution of atmospheric radars.

Acknowledgments. We thank the technical staff of the SOUSY research group, especially Klaus Meyer and Godehard Monecke, for their assistance in collecting and processing the data presented in this work. We also thank Carlton Ulbrich of Clemson University for providing the software used in producing Figure 3. In addition we wish to acknowledge the other members of the SOUSY group for their comments and ideas in the development of the experiment. One of us (PBC) was supported by the Max-Planck-Gesellschaft zur Förderung der Wissenschaften.

References

Awe, O., Errors in correlations between time series, *J. Atmos. Terr. Phys.*, *26*, 1239–1255, 1964.

Chu, Y.-H., and S. J. Franke, A study of the frequency coherence of stratospheric and tropospheric radar echoes made with Chung-Li VHF radar, *Geophys. Res. Lett.*, *18*, 1849–1852, 1991.

Dalaudier, F., C. Sidi, M. Crochet, and J. Vernin, Direct evidence of "sheets" in the atmospheric temperature field, *J. Atmos. Sci.*, *51*, 237–248, 1994.

Doviak, R. J., and D. S. Zrnić, Reflection and scatter formula for anisotropically turbulent air, *Radio Sci.*, *19*, 325–336, 1984.

Franke, S. J., Pulse compression and frequency domain interferometry with a frequency-hopped MST radar, *Radio Sci.*, *25*, 565–574, 1990.

Franke, S. J., J. Röttger, and C. LaHoz, Frequency domain interferometry of polar mesosphere summer echoes with the EISCAT VHF radar: A case study, *Radio Sci.*, *27*, 417–428, 1992.

German Meteorological Service, Aerological Diagrams for October 6 and 7, *Eur. Meteorol. Bull.*, *19*, 1994.

Kilburn, C., S. Fukao, and M. Yamamoto, Frequency domain interferometry on the MU radar using two pairs of frequencies, in *STEP Handbook*, pp. 258–262, SCOSTEP Secr., Natl. Oceanic and Atmos. Admin., Boulder, Colo., 1994.

Kudeki, E., and G. R. Stitt, Frequency domain interferometry: A high-resolution radar technique for studies of atmospheric turbulence, *Geophys. Res. Lett.*, *14*, 198–201, 1987.

Kudeki, E., and G. R. Stitt, Frequency domain interferometry studies of mesospheric layers at Jicamarca, *Radio Sci.*, *25*, 575–590, 1990.

Palmer, R. D., R. F. Woodman, S. Fukao, M. F. Larsen, M. Yamamoto, T. Tsuda, and S. Kato, Frequency domain interferometry observations of tropo/stratospheric scattering layers using the MU radar: Description and first results, *Geophys. Res. Lett.*, *17*, 2189–2192, 1990.

Palmer, R. D., M. F. Larsen, C. J. Heinselman, and I. S. Mikkelsen, Frequency domain interferometry using the 1290 MHz Søndre Strømfjord radar: First results, *J. Atmos. Oceanic Technol.*, *10*, 618–632, 1993.

Pan, C. J., C. H. Liu, and J. Röttger, Refined method of frequency domain interferometry for the MST radar, in *STEP Handbook*, pp. 239–241, SCOSTEP Secr., Natl. Oceanic and Atmos. Admin., Boulder, Colo., 1994.

Schmidt, G., R. Rüster, and P. Czechowsky, Complementary code and digital filtering for detection of weak VHF radar signals from the mesosphere, *IEEE Trans. Geosci. Electron.*, *17*, 154–160, 1979.

Stitt, G. R., and E. Kudeki, Interferometric cross-spectral studies of mesospheric scattering layers, *Radio Sci.*, *26*, 783–799, 1991.

P. B. Chilson and G. Schmidt, Max-Planck-Institut für Aeronomie, Postfach 20, D-37189 Katlenburg-Lindau, Germany. (e-mail: chilson@linaxl.mpae.gwdg.de)

(Received May 31, 1995; revised August 31, 1995; accepted November 17, 1995.)